Astron. Astrophys. 332, 1044–1054 (1998)

ASTRONOMY AND ASTROPHYSICS

Hydrodynamical models of planetary nebulae and the problem of abundance determinations

M. Perinotto[1], **K. Kifonidis**[1,2,3], **D. Schönberner**[2], **and H. Marten**[2,⋆]

[1] Dipartimento di Astronomia e Scienza dello Spazio, Largo E. Fermi 5, I-50125 Firenze, Italy
[2] Astrophysikalisches Institut Potsdam, Telegrafenberg, D-14473 Potsdam, Germany
[3] Max-Planck-Institut für Astrophysik, Karl-Schwarzschild-Strasse 1, D-85740 Garching, Germany

Received 18 June 1997 / Accepted 6 October 1997

Abstract. The problem of the accuracy that can be attained in the derivation of chemical abundances in Planetary Nebulae (PNe) with the best techniques of the "constant $T_{\rm e}$, $n_{\rm e}$" type currently in use, has been considered. This has been done by constructing two sequences (A, B) of radiation-hydrodynamical PNe models under the framework of the interacting stellar-winds theory which are intended to represent real planetaries in different evolutionary stages. Both sequences evolve along the 0.605 $M_{\odot}$ stellar evolutionary track of Blöcker (1995b), but start from different initial conditions. Corresponding equilibrium models were also computed for a number of specific models along the stellar track to obtain an estimate of the errors that would result from stationary PNe models.

The line intensities calculated from these models are interpreted under the scheme of the "constant $T_{\rm e}$, $n_{\rm e}$" method and the derived elemental abundances are compared with the original input values. The obtained deviations vary for the different elements. In the optically thin cases the discrepancies between the abundances derived using the "constant $T_{\rm e}$, $n_{\rm e}$" method and the corresponding input values amount to less than 10% for helium and to maximum factors of 1.5 to 3 for oxygen, nitrogen, neon and argon. The discrepancy is higher for sulphur, reaching an order of magnitude in the most excited models. Particular attention has to be given to optically thick models. It is found that the "constant $T_{\rm e}$, $n_{\rm e}$" method can yield rather erroneous results in these cases. Only minor deviations are found between abundances calculated from the hydrodynamical models and those in equilibrium.

Key words: chemical abundances – planetary nebulae – hydrodynamics – stellar evolution

1. Introduction

The physical processes governing line formation in stationary gaseous nebulae are believed to have been well established for a long time (Seaton 1960; Spitzer 1978; Osterbrock 1974, 1989; Aller 1984; Harrington 1989). The determination of chemical abundances, particularly in Planetary Nebulae (PNe) with their relatively high degree of symmetry and small amount of dust grains, has therefore been considered to be rather safe (cf. Kaler 1985; Pottasch 1984a). Discussion of their implications for the theory of stellar evolution has been quite extensive (Iben & Truran 1978; Iben & Renzini 1983; Iben 1984; Renzini & Voli 1981; Marigo et al. 1996). In comparison with the predictions of the stellar evolution theory it is of course of paramount importance to be able to define the accuracy which is attached to each individual determination of chemical abundances, something which, in our opinion, is currently not handled with a sufficient care. We also note that in principle a dynamical treatment is needed, considering the complicated velocity field, the density structure and the occurrence of shocks within a planetary. The importance of an accurate knowledge of the chemical abundances is clear already in connection with the simple, yet very important question, on whether a given PN is carbon or oxygen rich. Only a precise knowledge of the accuracy of the measured C/O abundance ratio permits derivation of meaningful astrophysical conclusions from the observed distribution of C/O in PNe. Similarly an accurate knowledge of the errors of chemical abundances is required when dealing with abundance gradients from PNe in galaxies.

It is useful to recall that the determinations of chemical abundances in PNe are done with three methods:

i) by comparing individual line fluxes with those predicted from detailed photoionization models;
ii) by approximating the nebula with one, two or more zones (with $T_{\rm e}$, $n_{\rm e}$ constant in each zone) and using a proper ionization correction scheme for the unseen ions;
iii) with a procedure intermediate between the first two. (a) The ionic abundances are first derived from the observed line fluxes, as in ii); (b) a photoionized model is tailored for the

Send offprint requests to: M. Perinotto

⋆ *Present address:* Forschungszentrum Karlsruhe GmbH, Institut für Neutronenphysik und Reaktortechnik, Postfach 3640, D-76021 Karlsruhe, Germany

specific nebula, reproducing relevant intensity line ratios, as the one from O^{2+}/O^{+} ions; (c) icf's are then derived from (b) and used to get total abundances from (a).

Technique iii) was used essentially by Aller and associates (Aller & Czyzak 1983; Aller & Keyes 1987) on about 90 PNe. Method i), which is physically the most satisfactory, has been applied to very few objects so far. The bulk of our information rests on method ii) (in its different specifications), used for the determination of abundances in more than 250 galatic PNe. When properly applied, method ii) may produce chemical abundances not far from those of method i) (cf. Pottasch 1984b). Based on a comparison of results from the different methods on the well studied planetary NGC 7662, Pottasch emphasizes: "A tentative conclusion is that careful analysis using the constant $T_{\rm e}$, $n_{\rm e}$ method will give abundances within 30% to 50% of the results of the detailed nebular models. It is likely that the absolute accuracy of the abundances from nebular models is also limited to 30–50% because of a combination of various factors discussed above."

To assess the general validity of these concepts, a more extended use of method i) is clearly desirable. But there are limitations because this method requires various poorly known information items, including the distance of the object. In other words one is dealing with a multi-parameter problem, with the possibility of non-unique solutions.

The comparison of the abundance of a given ion as derived by lines powered by different physical processes is clearly quite important to assess the correctness of the derived abundances. A well known example is the abundance of C^{2+}, which is much larger if the faint recombination line 4267 Å is used, relative to the value derived from the strong collisionally excited 1909 Å C III] semiforbidden doublet. Efforts to explain the discrepancy in terms of some other mechanism, as fluorescence from the central star, contributing to the population of the upper level of the 4267 Å transition did not provide a solution. Waiting for an explanation, the general wisdom has been to give credit to the lower values derived from the well observed 1909 C III] doublet. Recently the same type of difficulty arose again with the abundance of O^{2+}, when detailed calculations of the recombination coefficients of the O^{+} permitted lines in the optical became available (Péquignot et al. 1991; Osterbrock et al. 1992; Peimbert et al. 1993; Storey 1994). One possibility invoked to alleviate the problem is a significant role of the so-called "temperature fluctuations", discussed by Peimbert (1967). According to this description, the temperature to be used to deduce the abundance of O^{2+} (and of other ions as well) is not the one directly derived from the classical 4363/5007 line ratio, but a smaller one. With this lower temperature the deduced abundance is higher, closer to the value from the (temperature independent) recombination lines. Liu et al. (1995) found however that this effect is not sufficient to explain the discrepancy, which amounts up to a factor of five in NGC 7009. On the other hand, recent work by Rubin et al. (1997) making use of far-infrared emission lines, which are quite insensitive to the electron temperature, appears to confirm the oxygen abundance derived for NGC 7009 from the classical UV/optical collisionally excited lines.

All in all, it is evident that substantial work needs to be done to come to a satisfactory understanding of the errors associated with the determinations of chemical abundances in PNe. With the present work, we wish to contribute to the subject by evaluating the errors that can be associated to the determinations made with method ii) just due to the basic assumption of constant electron density and temperature. While this is only a piece of the effort to be made, it will at least serve to give a quantitative idea of errors inherent in method ii) and therefore in the bulk of the available abundances in PNe.

In Sect. 2 we illustrate the modeling of the planetary nebulae and the technique used to derive abundances. The results are presented and discussed in Sect. 3. The conclusions follow in Sect. 4.

2. Modeling planetary nebulae and abundances determinations

To investigate the issue of abundance determinations in planetaries we proceed in two steps: in the first one hydrodynamical models are calculated with assigned input chemical abundances which serve as substitutes of real planetaries. This first step contains two items:

i) radiation gasdynamical modeling along theoretical stellar evolutionary tracks in the HR diagram in the framework of the interacting-winds theory;
ii) generation of "equilibrium" models from selected models of the hydrodynamical sequences, which are equivalent to stationary photoionization models.

The second step contains the determination of the chemical abundances with the "constant $T_{\rm e}$, $n_{\rm e}$" method and their comparison with the input values. It will then provide us with information on the errors inherent in this method.

2.1. The physical model

It is an established fact that a PN forms out of the envelope the central star looses during its evolution on the asymptotic giant branch (AGB) due to slow but massive stellar winds. Unfortunately, to date neither observations nor theoretical models can provide a final picture of the mass loss history on the AGB for given stellar parameters. On the theoretical side there seems to be some consensus that pulsationally induced shock waves in connection with dust formation are the driving force of the winds. The subsequent radiative acceleration of the grains and their momentum coupling to the gas can account for the observed mass loss rates and velocities. Despite the substantial progress that has been made in the self-consistent modeling of such winds during the last few years (see e.g. Fleischer et al. 1995; Höfner et al. 1995 and the references therein) one is far from incorporating such models into stellar evolutionary calculations. The latter is, however, needed to derive the resulting density distribution of the circumstellar shell at the end of the AGB phase from first principles. This density structure is the crucial initial quantity needed for the computation of realistic radiation gasdynamical models of PNe. It has, in general, still to

be prescribed assuming a stationary outflow and different mass loss phases on the AGB (see also Sect. 2.3).

According to the interacting stellar-winds model (Kwok et al. 1978) this slow wind is hit by the tenuous but fast, radiation-driven wind emitted by the central star during its evolution towards white dwarf dimensions. The terminal velocity of this fast outflow increases with the shrinking stellar size and therefore the character of the flow pattern that results in the interaction with the slow wind changes with time.

The properties of the stellar wind in the early phases of post-AGB evolution are rather uncertain. The mass loss rate should, however, decrease in this period from the values characteristic of dust-driven AGB winds ($10^{-5} \ldots 10^{-4}$ $M_\odot$/yr) to the ones of hot radiation driven winds which in the case of planetary nebulae nuclei are of the order of 10^{-8} $M_\odot$/yr. The velocity on the other hand is expected to increase from about 10 km/sec to more than 1000 km/sec. As long as its value is small (of the order of 100 km/sec) a nearly isothermal shock forms in the interaction region; i.e. the thermalized mechanical energy of the fast wind is effectively radiated away in the dense cooling region behind the shock front. This is the so called "momentum conserving" phase of the wind interaction.

However, the fast wind's increasing velocity will quickly (i.e. within a few hundred years) lead to a situation where radiative cooling in the expanding and diluting gas can no longer compete with the increasing mechanical energy input. When this happens, a zone of hot, low-density gas forms behind the shock. This high-temperature region – also called the "hot bubble" – is separated by a contact discontinuity from the slow wind and sweeps up the actual dense nebular shell. The latter is bounded on its outer rim by a second shock which separates the swept-up gas from the rest of the slow wind material (the "halo" in the following). This "energy conserving" form of wind interaction then prevails for the largest part of a typical PN's life.

Already Schmidt-Voigt & Köppen (1987) – and later Marten & Schönberner (1991) and Mellema (1994) – have shown that this picture of PN evolution is incomplete. Using stellar models with masses of about 0.6 $M_\odot$ evolving along recent evolutionary tracks these PNe models made clear that for densities typically found in the circumstellar shells of AGB stars the onset of hydrogen photoionization leads to strong dynamical effects in the early evolutionary phases: a D-type ionization front forms in the slow wind which drives a shock into the neutral gas ahead of it long before an outer shock resulting from wind interaction can form. The effects of photoionization must therefore be included in hydrodynamical computations as well as a great number of cooling processes. Finally, Marten (1994, 1995) has shown that the evolutionary time scale of the central star may become comparable to the heating/cooling and ionization/recombination time scales of the gas, so that even a fully time-dependent treatment of the ionization and energy balance may become necessary.

Only a self-consistent radiation gasdynamical description of all the processes mentioned can lead to a reliable modeling of PN evolution. Numerically, this is a difficult task since it results in an ionization rate network for a large number of ions which has to be solved together with the hydrodynamics. For a self-consistent computation of the cooling caused by collisonally excited lines – which yields the main contribution to the loss of thermal energy – this system has to be supplemented by the equations of statistical equilibrium for a large number of transitions. We have used a newly developed radiation gasdynamical code to compute our PNe models which will be outlined in the next section.

2.2. The radiation gasdynamical code

Since a detailed description of the code and a discussion of the results obtained with it so far is given elsewhere (Marten & Szczerba 1997; Schönberner et al. 1997; Schönberner et al., in prep.), we only mention here some basic aspects. Our code solves the Eulerian equations of hydrodynamics supplemented by the continuity equations for the single particle densities in spherical symmetry

$$\frac{\partial \boldsymbol{Q}}{\partial t} + \frac{\partial \boldsymbol{F}}{\partial r} = \boldsymbol{S}, \tag{1}$$

with state- and flux-vectors, $\boldsymbol{Q}$ and $\boldsymbol{F}$, respectively given by

$$\boldsymbol{Q} = \begin{pmatrix} \varrho \\ \varrho v \\ e \\ n_{\rm e} \\ n^{\beta,l} \end{pmatrix}, \quad \boldsymbol{F}(\boldsymbol{Q}) = \begin{pmatrix} \varrho v \\ p + \varrho v^2 \\ (p+e)v \\ n_{\rm e} v \\ n^{\beta,l} v \end{pmatrix} \tag{2}$$

and the geometrical source terms

$$\boldsymbol{S} = -\frac{2v}{r} \begin{pmatrix} \varrho \\ \varrho v \\ p + e \\ n_{\rm e} \\ n^{\beta,l} \end{pmatrix}. \tag{3}$$

All quantities have their usual meanings with $e = e_{\rm th} + \frac{1}{2}\varrho v^2$ denoting the total advected energy density (made up of a thermal and a kinetic part), $n^{\beta,l}$ the particle density for the ion of species β and ionization state l, and $n_{\rm e}$ the electron density. The energy stored in the ionization state of the gas does not need to be advected explicitely since this is already accounted for by the separate advection of the single ion densities. In order to account for the strong shocks and to minimize numerical diffusion across the contact discontinuity a high-resolution, second-order Godunov-type advection scheme (LeVeque 1997) including a Riemann solver is used for the integration of Eq. (1). The equation of state is that of an ideal gas.

A *fully time-dependent* ionization rate network given by the system of ordinary differential equations

$$\frac{d}{dt} n^{\beta,l} = R_{\beta,l}, \quad \forall \beta, l \tag{4}$$

$$\frac{d}{dt} e_{\rm th} = G - L - \sum_{\beta} \sum_{l=2}^{N_\beta} R_{\beta,l} \sum_{k=2}^{l} \chi_{\beta,k-1}, \tag{5}$$

along with the particle conservation of species β

$$\sum_{l=1}^{N_\beta} R_{\beta,l} = 0, \quad \forall\beta \tag{6}$$

and the condition of charge neutrality

$$n_{\rm e} = \sum_{\beta} \sum_{l=1}^{N_\beta} (l-1) n^{\beta,l} \tag{7}$$

is solved implicitly in step with the hydrodynamics to account for the source terms of the thermal energy and particle densities originating from heating/cooling and ionization/recombination processes. Here $R_{\beta,l}$ is the net rate for ion (β, l). It includes contributions due to photo- and collisional ionizations, radiative and dielectronic recombinations as well as charge-exchange reactions. See Marten & Szczerba (1997) for a detailed description of all terms including the total energy gain, G , the total energy loss of the gas, L , and the last term on the rhs. of Eq. (5) which describes cooling by collisional ionizations (with $\chi_{\beta,l}$ denoting the ionization potential of ion (β, l)). Currently, up to 76 ions of the elements H, He, C, N, O, Ne, S, Cl and Ar, up to the ionization stage XII, are accounted for. Ionizations are always assumed to take place from the ground state of the respective ions. Radiative cooling is computed self-consistently and includes thermal bremsstrahlung, contributions due to recombinations, collisionally excited transitions of H^0 and up to approximately 300 collisionally excited lines of heavy ions.

The local mean intensity of the ionizing radiation field, J_ν, which enters into Eqs. (4) and (5) via the net rate $R_{\beta,l}$ consists of two terms: the geometrically diluted and exponentially weakened radiation field of the star, and a second term which represents the diffuse radiation field $J_\nu^{\rm d}$:

$$4\pi J_\nu(r) = \pi F_\nu^*(R_*) \left(\frac{R_*}{r}\right)^2 \exp\{-\tau_\nu(r)\} + 4\pi J_\nu^{\rm d}(r). \tag{8}$$

Only contributions due to the opacity caused by the photoionizations were considered in the optical depth τ_ν. Radiative transfer is solved for photon energies between 4 and 500 eV on a frequency grid containing up to 344 grid points in case the full network of 76 ions is used. The diffuse field $J_\nu^{\rm d}$ is treated in the "on the spot" approximation (Osterbrock 1989).

As already implied by writing the fully coupled radiation gasdynamical equations in the form (1), (4) and (5) an operator splitting technique is used to advance the solution of the full system numerically in time by alternating between the integration of the advection step Eq. (1) and the solution of the radiative sources Eqs. (4) and (5) along the radial grid. This, apart from simplifying code design, development and testing, has the advantage that it easily allows us to compute the relaxation of a full radiation hydrodynamical model to thermal and ionization equilibrium. The procedure employed for this purpose will be described in Sect. 2.4.

The computational domain usually has to cover three orders of magnitude in radius (from about 10^{15} up to $3 \cdot 10^{18}$ cm) in order to be able to follow the evolution from the instant when the star leaves the AGB up to the late stages when it evolves along the white dwarf cooling track. Since a rather high resolution is necessary in the nebula proper for an accurate treatment of the radiative transfer and the time dependent ionization problem (see Marten & Szczerba 1997), we used a constant distance ratio mesh with 1000 grid points for the calculations described below. The size of a mesh cell increases from 10^{15} cm at the inner to about five times that value at the outer grid boundary since high resolution is not necessary in the outer parts of the halo. But still, the large number of mesh points resulted in long computing times. In the late evolutionary stages the increasing velocity of the fast wind, which constitutes our inner boundary condition, even worsens the situation since it leads to very small time steps due to the Courant-Friedrichs-Levy stability condition. Our problem poses extreme difficulties for an explicit hydrodynamics scheme on a fixed Eulerian grid. Clearly, adaptive mesh refinement will become a necessity in future computations, especially for large scale parameter studies and the extension of the calculations to two spatial dimensions. Alternatively, an implicit adaptive grid method may turn out to be of benefit for the 1D-case. This would require major code changes and introduce large complexity both in code design and use, though. To our knowledge no implicit adaptive grid method has been coupled to such large ionization networks, yet.

2.3. Radiation gasdynamical models

Two different radiation gasdynamical PNe model sequences (Schönberner et al. 1997; Schönberner et al., in prep.) computed along the 0.605 $M_\odot$ stellar evolutionary track of Blöcker (1995b) were used for our investigations.

The first sequence (hereafter termed sequence A) has been computed with initial conditions basically taken from the three-wind-model of Marten & Schönberner (1991), the only difference being the assumption of a constant wind velocity of 15 km/sec for both the AGB wind and the superwind phase (see also Marten 1994). All nine elements and the full network of 76 ions were included into these computations.

In an attempt to estimate the effects of a more realistic initial density and velocity distribution on our results a second PN model sequence (B in the following) was taken from Schönberner et al. (1997). As described therein it is the result of a first attempt to follow the hydrodynamical evolution of a circumstellar shell from the AGB towards a planetary nebula. A combination of (parameterized) mass loss rates as used in recent stellar evolutionary calculations (Blöcker 1995a) with time-dependent hydrodynamical modeling of the resulting gas/dust-shell and subsequent computation of the PN evolution was used for this purpose. The elements included in these computations were H, He, C, N, O and Ne and with each ionization stage considered. In either case the slow wind is assumed to be initially neutral.

The spectral photon flux distribution was determined from the stellar effective temperature under the assumption of a black body spectrum. The velocity and mass loss rate of the fast cen-

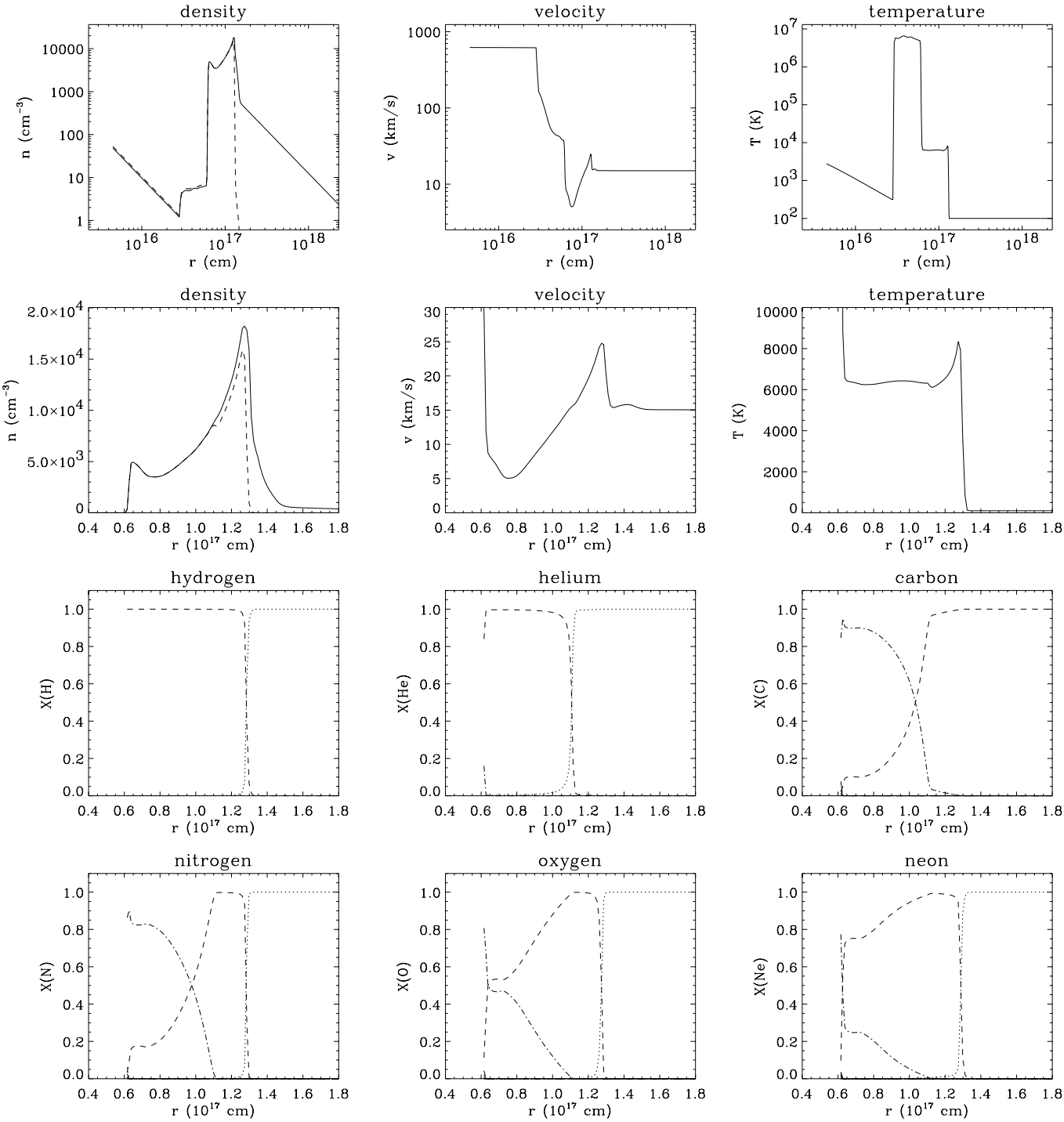

Fig. 1. The dynamical model belonging to instant A0 (t = 1796.87 yrs, $T_{\rm eff}$ = 28 886 K, L = 6299 $L_\odot$). The three upper panels show the hydrodynamical structure over the largest part of the computational grid while the remaining ones give a detailed picture of the actual nebula itself. The total ion density as well as the electron density (dashed curve) are depicted in the density plots. The following line styles are used for the ionization fractions: dotted: neutrals, dashed: singly ionized ions, dashed-dotted: doubly ionized ions, dashed-three-dotted: triply ionized ions. Note the hot bubble in the temperature plot of the third upper panel and the shock caused by the D-type ionization front at a radius of about $1.3 \cdot 10^{17}$ cm.

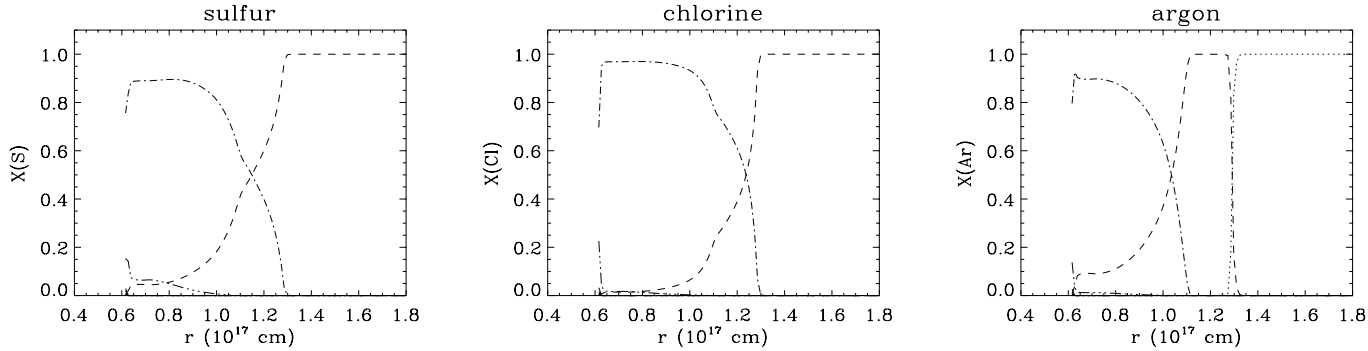

Fig. 1. (continued)

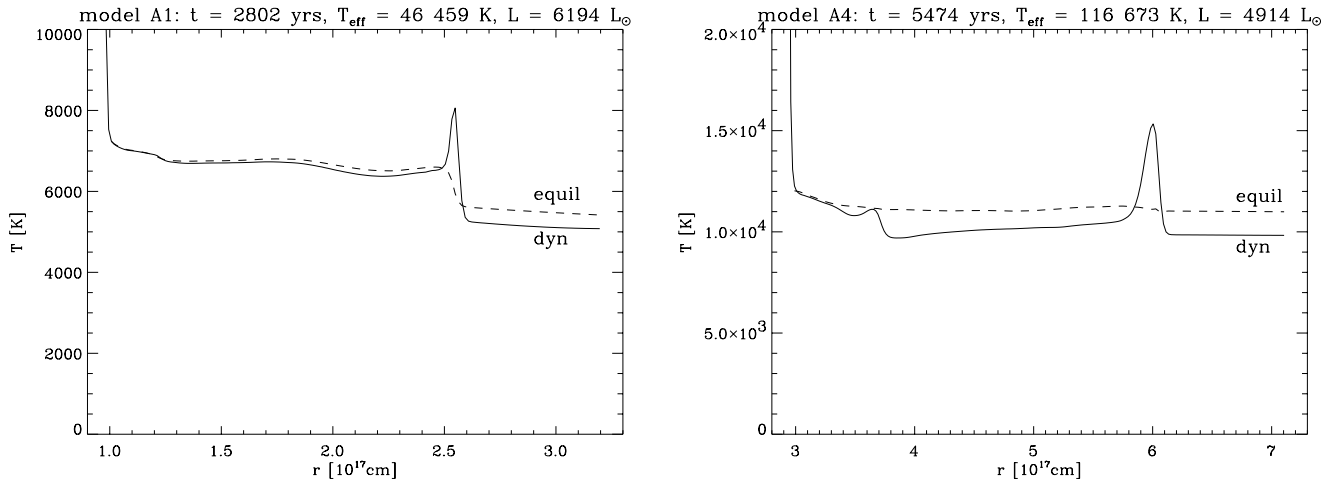

Fig. 2. Temperature structure of two optically thin models from sequence A. The actual nebula is bounded by the contact discontinuity at the inner rim, where the temperature jumps to the values encountered in the hot bubble, and a nearly isothermal shock at the outer rim (local temperature maximum at $r \approx 2.5 \cdot 10^{17}$ cm and $r \approx 6 \cdot 10^{17}$ cm for models A1 and A4 respectively). Beyond the latter extends the halo. Note that deviations from the corresponding equilibrium models become the more important the lower the density is, i.e. they are most apparent in the halo and in the model with larger age.

tral star wind were computed from the analytical approximation to the radiation driven wind theory as given by Kudritzki et al. (1989), with the line-force parameters suggested by Pauldrach et al. (1988). In the lower effective temperature range (below about 25 000 K) where the theory of radiation driven winds is not applicable we used the interpolation described in Marten & Schönberner (1991). The dynamical impact of the stellar wind is rather unimportant in this transition region, making a more sophisticated description not really necessary. Finally, we wish to emphasize that the post-AGB mass loss rates used in our models are the same as those in the calculations of Blöcker (1995b), thus avoiding inconsistencies between stellar and nebular evolution.

The first models of each sequence, i.e. models A0 and B0 (cf. Tables 2 and 3) represent nebulae that are optically thick in the Lyman continuum of hydrogen while the remaining models are optically thin. The elemental abundances given in Table 1 were used for all computations. We did *not* consider any temporal changes in the chemical composition of the gas expelled from the star.

Table 1. Elemental abundances used for the computation of our hydrodynamical models given on a logarithmic scale

H	He	C	N	O	Ne	S	Cl	Ar
12.00	11.04	8.89	8.39	8.65	8.01	7.04	5.32	6.46

2.4. Equilibrium models

The full radiation hydrodynamical models described in the previous sections differ from static photoionization models used in classical methods of abundance determinations in several respects:

a) they have a density structure consistent with the evolutionary state of the central star whereas in static photoionization models usually some form of simple density structure is assumed;
b) they include additional physical processes: viz. heating behind shocks and expansion cooling which lead to deviations from the equilibrium temperature;

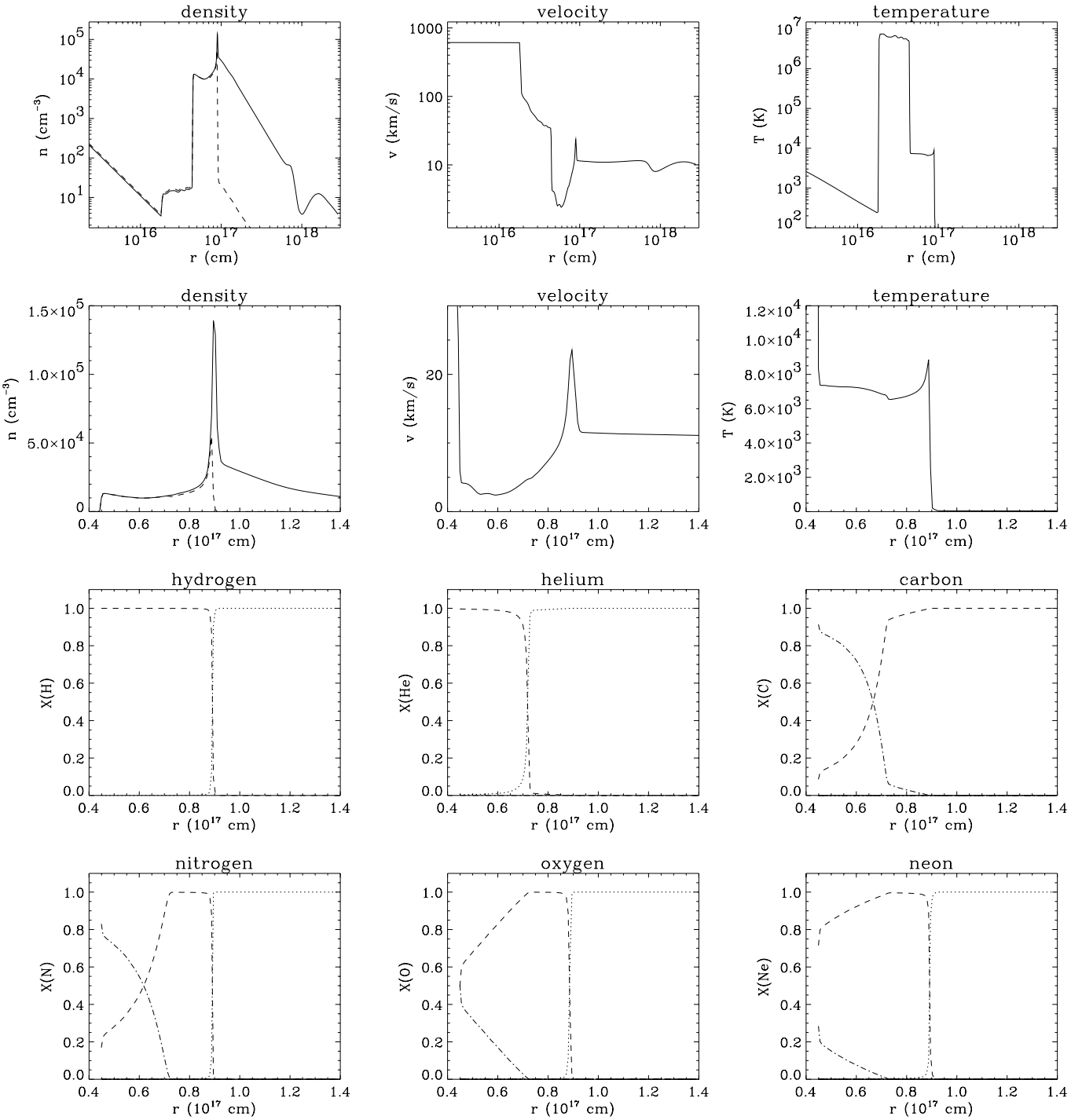

Fig. 3. Complete radial structure of our dynamical model belonging to instant B0 (t = 1776.54 yrs, $T_{\rm eff}$ = 28 561 K, L = 6299 $L_{\odot}$). Note the very high density behind the outer shock accompanying the D-Front compared to model A0. Otherwise, qualitatively the same structures as in the latter case are visible. The density dip near a radius of 10^{18} cm is a result of the temporarily decreased mass loss rate which followed the last thermal pulse on the AGB.

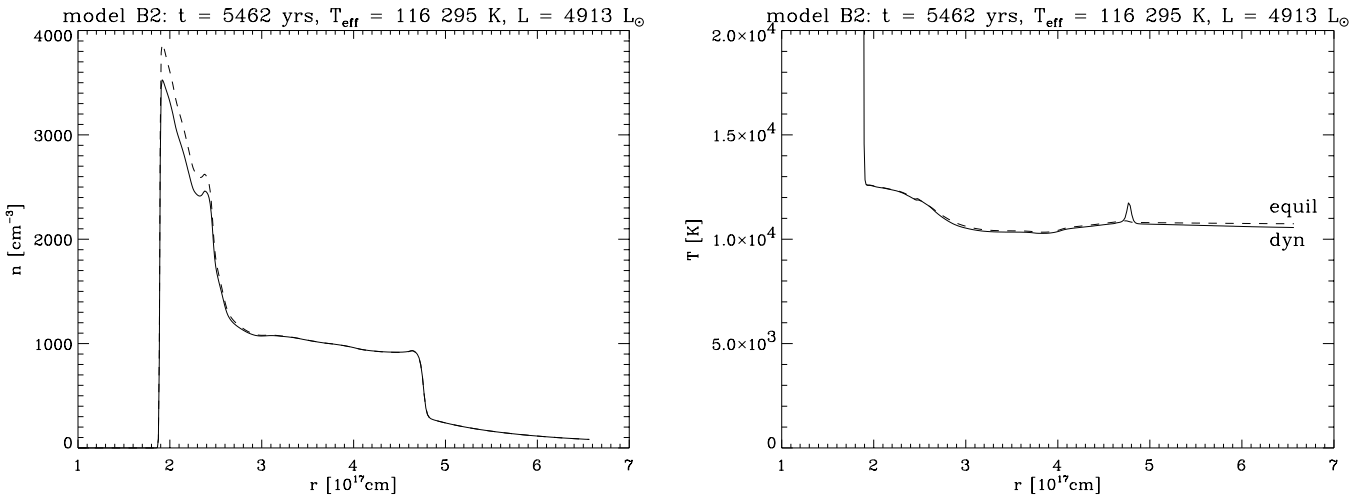

Fig. 4. Left: Total ion and electron density (solid and dashed lines respectively) of our dynamical model B2. Note that compared to Fig. 3 the density has decreased appreciably and the spike caused by the D-Front at the outer rim has disappeared. The increased pressure of the hot bubble has meanwhile swept up a new shell at the inner rim. Right: Temperature structure of the same model compared to the corresponding equilibrium model. Deviations from the equilibrium temperature structure are negligible due to the relatively high densities of $n \gtrsim 1000$ cm^{-3} in the main nebula.

c) apart from dynamical effects, deviations from thermal and ionization equilibrium can also result if the evolutionary time scale of the central star becomes comparable to the heating/cooling and ionization/recombination time scales of the gas, so that the time-derivatives in Eqs. (4) and (5) become important (see Marten 1995).

To estimate the effects of items b) and c) on the line fluxes, corresponding equilibrium models were computed for a number of our dynamical models along the central star's track. Using a given radiation hydrodynamical model as initial condition the luminosity and effective temperature of the star were fixed and the advection step Eq. (1) "switched off", i.e. the velocity, v, was set to zero everywhere on the grid. Then, only Eqs. (4) and (5) describing the radiative sources were solved until the time-derivatives vanished in the spatial regions of interest, i.e. the temperature and ionization structures are relaxed to their equilibrium values.

This procedure was carried out for the actual high-density nebula, where essentially all of the line radiation is formed, and a part of the surrounding low-density halo (see Figs. 2 and 4). The computational grid of the dynamical models extends farther in and outwards than shown in Figs. 2 and 4 but the method becomes numerically very expensive in regions of low densities, where the corresponding time scales for relaxation become large. To avoid long computing times one could of course compare the dynamical models directly to models obtained from a static photoionization code using the density structures of the dynamical models as input to the former. However, we refrained from such a procedure in order to avoid systematic errors which would almost inevitably result by the use of two distinct codes due to differences in atomic data, physical approximations and numerical methods.

Figs. 2 and 4 give an impression of the temperature structures obtained. The deviations turned out to be quite small especially in model sequence B where the initial density distribution resulted in a nebula which is quite dense even when the central star has nearly reached its maximum temperature after 5462 years of evolution. Larger deviations are to be expected, however, for later evolutionary phases, at least for sequence A where the densities are lower (see also Marten 1995). In our new calculations which do not yet cover stages as late as the ones in Marten (1995), the line fluxes between equilibrium and dynamical models differed by only a few percent. Therefore, the use of the equilibrium models for the determination of the chemical abundances resulted in values comparable to those gained with the dynamical models (see Sect. 3.3).

2.5. Determination of the "observed" chemical abundances

As said in the Introduction, we restrict ourselves to determinations made with method ii). Among the various choices of the "constant T_e, n_e" method, we adopt the one made in the accurate many-objects study by Kingsburgh & Barlow (1994, KB in the following). This recent work is homogenous with respect to:

a) the set of recent atomic data, and
b) the adopted scheme of the ionization correction factors (updated relative to previous schemes).

We recall here the temperatures and densities used by us to derive the abundances of the various ions. The procedure follows the one used by KB except for the electron density which we have everywhere derived from the [S II] doublet while KB used [O II] or [S II]. It is evident that the procedure is rather more elaborate than the simple "constant T_e, n_e" statement appears to indicate. The temperature from the 5755/6584 [N II] line ratio for neutral and singly ionized species was used and

that from the 4363/5007 [O III] line ratio for all other ions with the following specifications. A temperature one third of the way between T_e(N II) and T_e(O III) was adopted for S^{2+} and Ar^{2+}. T_e(O III) + 1000 K was chosen for all triply ionized species, except for C^{3+}, where T_e(O III) + 650 K was used instead. T_e(O III) + 2270 K was taken for all 4-times ionized species. The neutral species were not used to derive the total elemental abundance. The reason is that fractions of neutrals, e.g. for oxygen or nitrogen, were assumed to be the same as that of neutral hydrogen, in which case final abundance ratios with respect to hydrogen would not be much affected, at least if the neutrals are of minor importance relative to the sum of the ionized species. Note that the density from low ionization species was used also for high ionization species. This is because the density from the [Cl III] and [Ar IV] doublets, although sometimes observed, is of much lower accuracy than that from the [O II] and [S II] stronger doublets. On the other hand a very precise density is not required when deriving abundances relative to hydrogen.

We have used the same lines used by KB (listed in their Table 8), except for the space UV lines, which we have omitted. These lines have not been observed in the vast majority of relatively well observed PNe (see e.g. the compilation by Perinotto 1991). When observed (by IUE), they cannot always be safely put on the same basis as the optical lines, because of the different entrance apertures of the IUE spectrographs relative to the ground optical instruments and because of lack of lines in common between the two sets of instruments. We have instead added the 9069, 9532 [S III] doublet lines which can be observed from the ground (with the same instrument used to acquire optical data). We have thus preferred in his work to limit our analysis in order for it to be adequate for objects well observed by ground-based instruments.

Both the hydrodynamical models already described and the procedure by KB just explained make use of very recent temperature dependent collision strengths of heavy ions. However, to avoid any effect of residual differences in the atomic data used, we have computed the line fluxes of the hydrodynamical models from their temperature, density and ionization structure using precisely the same atomic data subsequently employed in the calculations of the elemental abundances. These atomic data are those used of KB. A comparison with the line fluxes calculated directly with the hydrodynamical code did in fact show agreement in all cases to within a few per cent. From the line fluxes we get the "observed" elemental abundance presented in Tables 2 and 3 for sequences A and B, respectively.

We consider the abundances of He, N, O, Ne, Ar and S relative to Hydrogen. Carbon is omitted because it is not implemented in the present version of our code.

3. Results and discussion

From the Tables 2 and 3 it is seen that the abundances calculated following the prescriptions of the presently most elaborate "constant T_e, n_e" method deviate from the input abundances differently for the various elements.

3.1. Optically thin hydrodynamical models

We first consider the optically thin hydrodynamical models A1 to A4, B1 and B2. By comparing the abundances derived from these models with the original input ones we find in sequence A maximum deviations of 10% for helium and by factors of 0.8 to 1.2, 0.4 to 2.2, 0.4 to 0.9, 0.9 to 0.4, 0.7 to 0.06 for oxygen, nitrogen, neon, argon and sulphur, respectively, the largest deviations occurring in the most excited models. If most of these deviations would be attributed to the ionization correction scheme adopted for unseen ions, we might infer that systematically larger icf's should be appropriate for the more excited models.

3.2. Optically thick hydrodynamical models

In the optically thick models A0 and B0 we note larger deviations than in optically thin models. To be precise, in model A0 the observed abundances are underestimated by factors of 4.2, 1.6, 1.3 and 3.4 in helium, oxygen, nitrogen and neon, respectively; they are overestimated by a factor 1.5 in argon, while they turn out to be about correct in sulphur. In model B0 argon and sulphur are not present, because the models of sequence B were computed with six elements. The behaviour of the other elements is similar to the case of A0, namely: 5.2, 3.3, 1.8, 6.9 for He, O, N and Neon respectively.

These larger deviations are due to the approximations intrinsic to the "constant T_e, n_e" method which become worse in these cases. To clarify the matter we illustrate in Figs. 1 and 3 the full behaviour of the physical parameters and of the ionization structure of models A0 and B0.

Consider Fig. 1. A conspicuous density enhancement is present at a radial distance between 1.2 and $1.35 \cdot 10^{17}$ cm. This is caused by the well known dynamical behaviour of the D-type ionization front which has formed in the superwind and drives a shock into the neutral gas. The ratio H^+/H^0 decreases to a value of 0.5 at a radius of about $1.3 \cdot 10^{17}$ cm, while He^+/He^0 reaches 0.5 already at about $1.1 \cdot 10^{17}$ cm. Therefore, helium is essentially neutral across the zone of the density enhancement, while hydrogen is still substantially ionized up to the radius of the density enhancement peak. The relative helium abundance He/H is consequently not well approximated by the used expression:

$$\frac{\mathrm{He}}{\mathrm{H}} = \frac{\mathrm{He}^+ + \mathrm{He}^{2+}}{\mathrm{H}^+}. \qquad (9)$$

The amount of He^{2+} is negligible in this low excitation model, but the amount of not measurable He^0 is not compensated by the unseen H^0, as is assumed in Eq. (9). The expression (9) will therefore underestimate considerably the true helium abundance. Indeed our analysis gives $He^+/H^+ = 0.026$, equal to He/H, a factor 4.2 below the true abundance. Similar considerations enter, together with the role of the icf's correction factors, to explain the deviations found in the other chemical elements.

In model B0 we have an even more pronounced density enhancement in the outer nebula peaking at about $0.9 \cdot 10^{17}$ cm just in front of the hydrogen ionization. The ratio He^+/He^0 drops at

Table 2. Derived elemental abundances for models of sequence A. The calculated final abundances for helium are 0.062 and 0.080 for models A0dyn and A0equil, respectively (see text). The input abundances are given in the second column

		A0		A1		A2		A3		A4	
		t = 1797 yrs		t = 2802 yrs		t = 3766 yrs		t = 4598 yrs		t = 5474 yrs	
		$T_{\rm eff}$ = 28 886 K		$T_{\rm eff}$ = 46 459 K		$T_{\rm eff}$ = 67 400 K		$T_{\rm eff}$ = 89 702 K		$T_{\rm eff}$ = 116 673 K	
		L = 6299 $L_\odot$		L = 6194 $L_\odot$		L = 5985 $L_\odot$		L = 5593 $L_\odot$		L = 4914 $L_\odot$	
Ratio	abund	dyn	equil	dyn	equil	dyn	equil	dyn	equil	dyn	equil
He/H	0.110	0.026	0.026	0.109	0.109	0.106	0.106	0.0995	0.0995	0.101	0.101
(O/H) $\times 10^4$	4.47	2.72	3.28	4.33	4.48	3.98	4.21	5.50	5.69	4.37	4.61
(N/H) $\times 10^4$	2.45	1.90	1.89	1.06	1.10	1.32	1.37	4.24	4.37	5.34	5.61
(Ne/H) $\times 10^4$	1.02	0.303	0.373	0.98	1.02	0.798	0.850	0.598	0.619	0.373	0.391
(S/H) $\times 10^6$	11.0	9.78	9.83	7.87	7.97	2.09	2.15	0.948	0.957	0.693	0.717
(Ar/H) $\times 10^6$	2.88	4.30	5.16	2.52	2.55	1.94	2.02	1.80	1.85	1.21	1.26

Table 3. Derived elemental abundances for models of sequence B. The calculated final abundances for helium are 0.060 and 0.035 for models B0dyn and B0equil, respectively (see text). The input abundances are given in the second column

		B0		B1		B2	
		t = 1777 yrs		t = 3770 yrs		t = 5462 yrs	
		$T_{\rm eff}$ = 28 561 K		$T_{\rm eff}$ = 67 491 K		$T_{\rm eff}$ = 116 295 K	
		L = 6299 $L_\odot$		L = 5985 $L_\odot$		L = 4913 $L_\odot$	
Ratio	abund	dyn	equil	dyn	equil	dyn	equil
He/H	0.110	0.021	0.018	0.105	0.105	0.104	0.104
(O/H) $\times 10^4$	4.47	1.37	1.70	3.39	4.41	4.39	4.42
(N/H) $\times 10^4$	2.45	1.34	1.33	2.79	2.15	2.34	2.36
(Ne/H) $\times 10^4$	1.02	0.148	0.184	0.804	1.09	0.843	0.847

about $0.72 \cdot 10^{17}$ cm. Then, also in this case, helium is all neutral across the density enhancement where hydrogen is ionized up to the inner part of the density peak. The derived He^+/H^+ is 0.021 equal to He/H, since He^{2+} is negligible. Expression (9) underestimates here He/H by the factor 5.2. The deviations of the elements He, O, N and Ne all follow the behaviour of the corresponding ones in model A0, at slightly higher amounts.

For helium we can improve the calculated He/H in the low excitation models A0 and B0, by adopting the formula (15) by Peimbert and Torres-Peimbert (1977) that they used for the Orion nebula, instead of the above Eq. (9). The resulting He/H are 0.062, 0.080 for the A0dyn and A0equil models respectively, and 0.060, 0.035 for the corresponding B0 models. The discrepancy with the input values is thus reduced, although not completely.

From the above it is obvious that the errors inherent in the "constant $T_{\rm e}, n_{\rm e}$" method depend on the specific ionization stratification and density structure of the nebula. Our hydrodynamical models show that especially in the early evolutionary phases the latter is highly dependent on the adopted initial density distribution which in turn depends on the mass loss history on the AGB. For instance, in cases of rather small mass loss rates and/or high stellar luminosities it is to be expected that hydrogen ionization does not proceed via a D-type front at all. Instead, an R-type front should form, expanding supersonically relative to the neutral gas and causing only minor dynamical effects. Currently, no elaborate parameter study using realistic radiation gasdynamical PNe modeling with a large number of initial density distributions and stellar post-AGB tracks exists that adresses these questions. A small-scale study (Schönberner et al., in prep.) indicates, however, that – assuming a stationary outflow – the critical AGB mass loss rate for the formation of a D-type front amounts to about 10^{-5} $M_\odot$/yr for Blöcker's 0.605 $M_\odot$ central star. Since already the computation of sequences A and B required several thousand hours of CPU time, limited computational resources have forced us to refrain from probing abundance errors that would result from the "constant $T_{\rm e}$, $n_{\rm e}$" method when a larger number of initial density distributions and stellar tracks with different masses would be used.

3.3. Equilibrium versus hydrodynamical models

The differences in the abundances obtained from the full hydrodynamical and the equilibrium models were found to be always small both in the optically thin and in the optically thick models. The equilibrium abundances are almost always larger than the dynamical ones. In no case is the difference greater than 25 %.

As illustrated in Figs. 2 and 4 the temperature behaviour in the two types of models is similar, with T_e in the equilibrium models either equal to or a bit larger than that in the dynamical models, apart from the increase in the latter models at the outer nebular rim, due to heating behind the shock. This is however a local effect which does not affect significantly the abundances deduced with the "constant T_e, n_e" method. A higher electron temperature should result in smaller ionic abundances in collisionally excited heavy ions and in larger ionic abundances in the ions whose levels are dominated by recombination processes, i.e. hydrogen and helium. The resulting ionic abundance of heavy ions relative to hydrogen should then be smaller. The opposite is observed. In reality the different T_e behaviour is already accounted for in our procedure of computing the line intensities from the whole model nebula. Thus when we interpret these line intensities with the "constant T_e, n_e" method, we would not expect any systematic effect due to this cause. We have not been able to determine the origin of these effects which are anyhow rather small.

4. Conclusions

The obtained results simply reflect the state-of-the-art minimum accuracy that can be claimed for the derived abundances with the mentioned technique. It is obvious, however, that in real nebulae local fluctuations in the physical parameters including condensations of various kinds, not all of them represented in the models considered in the present work, will cause further "inaccuracies" in the abundances derived with the examined method. We conclude by emphasizing that particular attention has to be given to the derivation of the chemical abundances with the "constant T_e, n_e" method for optically thick nebulae.

References

Aller L. H., 1984, Physics of Thermal Gaseous Nebulae, Dordrecht: Reidel

Aller L. H., Czyzak S. J., 1983, ApJS 51, 21

Aller L. H., Keyes C. D., 1987, ApJS 65, 405

Blöcker T., 1995a, A&A 297, 727

Blöcker T., 1995b, A&A 299, 755

Fleischer A. J., Gauger A., Sedlmayr E., 1995, A&A 297, 543

Harrington J. P., 1989, in IAU Symp. 131. "Planetary Nebulae", Ed. S. Torres-Peimbert, Dordrecht: Reidel, p. 157

Höfner S., Feuchtinger M., Dorfi E. A., 1995, A&A 297, 815

Iben I. Jr., 1984, ApJ 277, 333

Iben I. Jr., Renzini A., 1983, ARA&A 21, 271

Iben I. Jr., Truran J.W., 1978, ApJ 220, 980

Kaler J. B., 1985, ARA&A 23, 89.

Kingsburg R. L., Barlow M. J., 1994, MNRAS 271, 257

Kudritzki R. P., Pauldrach A., Puls J., Abott D. C., 1989, A&A 219, 205

Kwok S., Purton C. R., Fitzgerald P. M., 1978, ApJ 219, L215

LeVeque R. J., 1997, Jour. Comp. Phys., in press

Liu X.-W., Storey P. J., Barlow M. J., Clegg R. E. S., 1995, MNRAS 272, 369

Marigo P., Bressan A., Chiosi C., 1996, A&A 313, 545

Marten H., 1994, PhD thesis, University of Kiel

Marten H., 1995, in "Asymmetrical Planetary Nebulae", A. Harpaz and N. Soker, Eds., Annals of the Israel Physical Society, Vol. 11, p. 273

Marten H., Schönberner, D., 1991, A&A 248, 590

Marten H., Szczerba R., 1997, A&A 325, 1132.

Mellema G., 1994, A&A 290, 915

Osterbrock D. E., 1974, Astrophysics of Gaseous Nebulae, S. Francisco: Freeman

Osterbrock D. E., 1989, Astrophysics of Gaseous Nebulae and Active Galactic Nuclei, University Science Books: Mill Valley, CA, USA

Osterbrock D. E., Tran H.D.,Veilleux S. 1992, ApJ 389, 305

Pauldrach A., Puls, J., Kudritzki R. P., Mendez R.H., Heap S. R., 1988, A&A 207, 123

Peimbert M., 1967, ApJ 150, 825

Peimbert M., Torres-Peimbert S., 1977, MNRAS 179, 217

Peimbert M., Storey P., Torres-Peimbert S., 1993, ApJ 414, 626

Perinotto M., 1991, ApJS 76, 687

Péquignot D., Petitjean P., Boisson C., 1991, A&A 251, 680

Pottasch S. R., 1984a, in "Planetary Nebulae: A Study of Late Stages of Stellar Evolution", Dordrecht: Reidel r

Pottasch S. R., 1984b, in "Planetary Nebulae: A Study of Late Stages of Stellar Evolution", Dordrecht: Reidel, p. 57

Renzini A., Voli M., 1981, A&A 94, 175

Rubin R.H., Colgan S.W.J., Haas M.R., Lord S.D., Simpson J.P., 1997, ApJ 479, 332.

Schmidt-Voigt M., Köppen J., 1987, A&A 174, 211

Schönberner D., Steffen M., Stahlberg J., Kifonidis, K., Blöcker, T., 1997 in "The Carbon Star Phenomenon", R. Wing Ed., Kluwer, in press

Seaton M. J., 1960, Rep. Progr. Phys. 23, 313

Spitzer L. Jr., 1978, "Physical Processes in the Interstellar Medium", New York: Wiley-Interscience

Storey P., 1994, A&A 282, 999

This article was processed by the author using Springer-Verlag LaTeX A&A style file *L-AA* version 3.